

**DIELECTRIC CONSTANT ESTIMATION FOR APOLLO 16 SITE USING MINI-RF SAR DATA.**

Y. Gao<sup>1,2</sup>, X. Liu<sup>1</sup>, W. Hou<sup>1,2</sup>, Y. Han<sup>1,2</sup>, H. Zhang<sup>1</sup> and R. Wang<sup>1</sup>. <sup>1</sup>Department of Space Microwave Remote Sensing System, Aerospace Information Research Institute, Chinese Academy of Sciences, Beijing, China, 100190 (gaoyao18@mails.ucas.edu.cn), <sup>2</sup>School of Electronic, Electrical and Communication Engineering, University of Chinese Academy of Sciences, Beijing, China, 100049.

**Introduction:** The dielectric constant of lunar regolith is of great significance for understanding the composition and evolution of lunar regolith and the distribution and content of mineral resources [1]. During the Apollo mission, a large number of samples of the lunar surface were collected on-site, and then the density and dielectric constant were measured in the laboratory [2]. Radar backscatter is sensitive to the physical parameters of planetary surface, such as dielectric constant and surface roughness [3]. Mini-RF aboard Lunar Reconnaissance Orbiter (LRO) and Mini-SAR aboard Chandrayaan-1 are lunar orbit hybrid compact polarimetric (HCP) synthetic aperture radar (SAR) that transmit circularly polarized electromagnetic waves and receive horizontal and vertical linear polarized echoes [4]. In fact, there have been a few studies on the inversion of the dielectric constant of lunar surface using polarimetric SAR data [3,5]. The X-Bragg model was first proposed in Earth remote sensing to retrieve surface roughness and dielectric constant using quadrature-polarimetric (quad-pol) SAR data [6]. It accounts for both cross-polarization and depolarization effects, which improve the application range of the model.

In this work, we extend the X-Bragg model to the processing of HCP SAR data by introducing the HCP similarity parameter. Then, the inversion of dielectric constant was performed for Apollo 16 site using Mini-RF SAR data, and the results were compared with the laboratory measurements sampled in the field.

**Methodology:** Mini-RF is designed to operate in two modes: baseline mode with a spatial resolution of 150 m and zoom mode with a spatial resolution of  $15 \times 30$  m. In this paper, the Stokes parameter products acquired in S-band (12.6 cm in wavelength) zoom mode are utilized.

Based on the relationship between the Stokes parameter of HCP SAR and the coherence matrix of quad-pol SAR [7], the  $\alpha$  parameter in X-Bragg model under HCP SAR can be obtained by

$$\alpha_{X-Bragg} = \frac{1}{2} \arctan \left( \frac{A_2 \sin c(2\beta_1)}{0.5(A_1 - 2A_3)} \right) \quad (1)$$

$$A_1 = |R_s + R_p|^2, \quad A_2 = (R_s + R_p)(R_s^* - R_p^*)$$

$$A_3 = \frac{1}{2} |R_s - R_p|^2$$

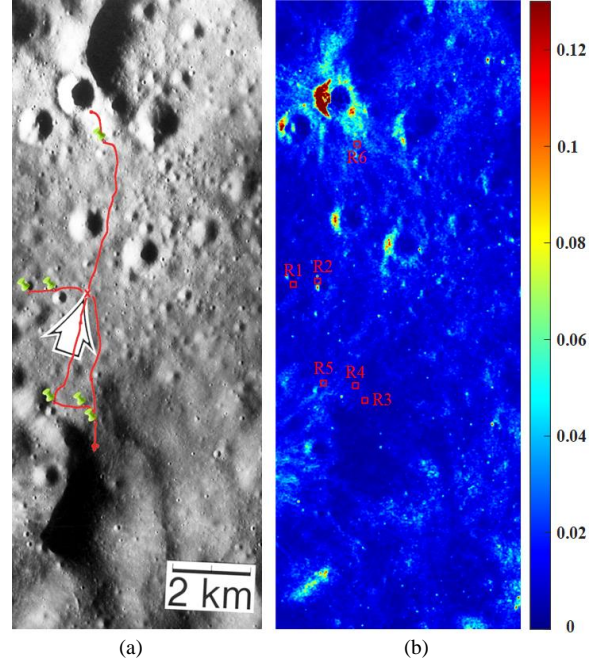


**Figure 1.** (a) High-resolution optical image of the Apollo 16 landing area (NASA AS16-4558), in which the red line indicates the exploration route; (b) Mini-RF S-band normalized radar backscatter intensity image covering the Apollo 16 landing area (LSZ\_06603\_2CD\_EKU\_14S016\_V1).

where  $R_s$  and  $R_p$  are the Bragg scattering coefficients related to the dielectric constant and radar incidence angle [6].  $\beta_1$  is related to the surface roughness, which cannot be obtained directly from HCP SAR data. Here, the similarity parameter of HCP SAR is introduced to calculate the scattering similarity between two scatterers, and then the  $\beta_1$  is estimated according to the magnitude of the similarity parameter. Similar to the scattering similarity parameter of quad-pol SAR [8], the similarity of two arbitrary  $2 \times 2$  HCP averaged wave coherence matrices  $C_1$  and  $C_2$  can be calculated by

$$r(C_1, C_2) = \frac{\text{Tr}(C_1 C_2^H)}{\text{Tr}(C_1) \text{Tr}(C_2)} \quad (2)$$

where  $\text{Tr}(\cdot)$  denotes the operation of matrix trace. From equation (2), it can be seen that the similarity parameter reaches a maximum value of 1 when  $C_1 = C_2$  and a minimum value of 0 when  $C_1$  is completely uncorrelated with  $C_2$ . It has been shown that the radar

echoes from smooth and flat surfaces will be dominated by the single scattering component [3]. Therefore,  $\beta_1$  can be estimated by calculating the similarity parameter between the coherence matrix of the Mini-RF radar echo and the coherence matrix of the standard single scattering mechanism. Then,  $\beta_1$  can be obtained by

$$\beta_1 = 1 - r \quad (3)$$

For a given Mini-RF radar image, the HCP similarity parameter is first calculated, which in turn yields the  $\beta_1$ . Then the  $\alpha$  parameter is obtained through the  $m$ - $\alpha$  decomposition [7]. At last, the value of dielectric constant can be acquired by equation (1). Before the inversion, a  $3 \times 3$  mean filter is employed to suppress the coherent speckle noise.

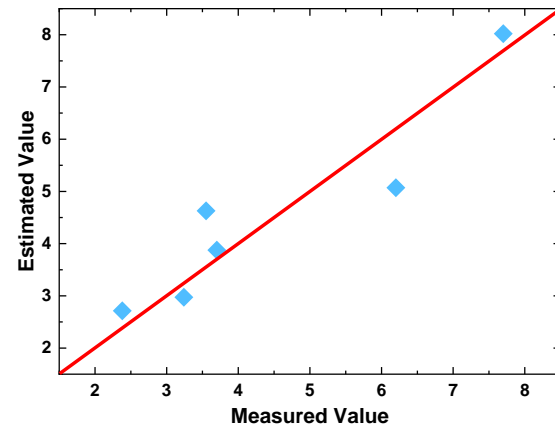
**Results and Analysis:** The landing and exploration of Apollo 16 mission were in the Descartes Highlands. The specific landing site was between North Ray and South Ray craters, which penetrated through the lunar regolith at the site, thus leaving exposed bedrock that could be sampled.

Fig. 1(a) shows the optical image of the Apollo 16 landing area, where the red line indicates the traverse route. Fig. 1(b) exhibits the Mini-RF S-band normalized radar backscatter intensity image of the landing area. As can be seen, there are lots of craters less than 1 km in diameter in this region, and the sampling is conducted around the crater ejecta. In Fig. 1(a), six sampling sites are selected to cover the lunar samples: 61500, 62295, 65015, 66055, 68121, 63501, and the corresponding regions are indicated by red rectangles on the Mini-RF image. Table 1 displays the details of the lunar samples corresponding to these six regions.

**Table 1.** Details of the lunar samples corresponding to the six selected regions [2].

	Station	Sample	Dielectric Constant
R1	Around Station 1	61500	3.55
R2	Around Station 2	62295	6.2
R3	Around Station 5	65015	7.7
R4	Around Station 6	66055	3.7
R5	Around Station 8	68121	3.24
R6	Around Station 13	63501	2.38

A  $9 \times 9$  window is selected in the Mini-RF image at the position corresponding to the above sampling point for dielectric constant inversion, and the average value is taken to obtain the final inversion result. Fig. 2 presents the relationship between the dielectric constant retrieved from the Mini-RF image and the laboratory measurements. It can be seen that the



**Figure 2.** Relationship between the dielectric constant retrieved from the Mini-RF image and the laboratory measurements of Apollo 16 samples.

estimated dielectric constants are quite close to the laboratory measurements with a determination coefficient ( $R^2$ ) of 0.87 and a root mean square error (RMSE) of 0.77.

The inversion results of the dielectric constant are an intermediate product, which can further provide supporting information for the classification of geological units, the distribution of mineral resources, and the detection of water ice in permanently shadowed areas. This paper provides a new way to estimate the dielectric constant of lunar surface using HCP SAR data, and the effectiveness is verified by inversion of the dielectric constant of Apollo 16 site. This paper is an initial result, and the performance of the proposed method will be evaluated in the future under more complex terrain conditions.

**Acknowledgments:** This work was supported by the National Science Fund for Distinguished Young Scholars under Grant 61825106 and the Beijing Municipal Natural Science Foundation under Grant 4192065. The authors are grateful to NASA Planetary Data System (PDS) Geosciences Node for providing Mini-RF SAR data.

**References:** [1] Papike J. J. et al. (1982) *Rev. Geophys.*, 20, 761-826. [2] Heiken G. H. et al. (1991) *Cambridge Univ. Press*, NY, USA. [3] Heggy E. et al. (2020) *Earth Planet. Sci. Lett.*, 541, 116274. [4] Raney R. K. et al. (2012) *JGR*, 117, E12. [5] Kumar A. et al. (2021) *IEEE Trans. Geosci. Remote Sens.*, Early Access. [6] Hajnsek I. et al. (2003) *IEEE Trans. Geosci. Remote Sens.*, 41, 727-744. [7] Cloude S. R. et al. (2012) *IEEE Geosci. Remote Sens. Lett.*, 9, 28-32. [8] Li D. et al. (2015) *IEEE Geosci. Remote Sens. Lett.*, 12, 2468-2472.